Mathematical Medicine and Biology Page 1 of 30
doi:10.1093/imammb/dqnxxx

The Influence of a Lipid Reservoir on the Tear Film Formation

KARA L. MAKI
School of Mathematical Sciences, Rochester Institute of Technology, 85 Lomb Memorial Drive, Rochester, NY 14625

RICHARD J. BRAUN
Department of Mathematical Sciences, University of Delaware, 15 Orchard Road, Newark, DE 19716

GREGORY A. BARRON
School of Mathematical Sciences, Rochester Institute of Technology, 85 Lomb Memorial Drive, Rochester, NY 14625

[Received on 20 June 2019]

We present a mathematical model to study the influence of a lipid reservoir, seen experimentally, at the lids margin on the formation and relaxation of the tear film during a partial blink. Applying the lubrication limit, we derive two coupled non-linear partial differential equations characterizing the evolution of the aqueous tear fluid and the covering insoluble lipid concentration. Departing from prior works, we explore a new set of boundary conditions enforcing hypothesized lipid concentration dynamics at the lid margins. Using both numerical and analytical approaches, we find that the lipid-focused boundary conditions strongly impact tear film formation and thinning rates. Specifically, during the upstroke of the eyelid, we find specifying the lipid concentration at the lid margin accelerates thinning. Parameter regimes that cause tear film formation success or failure are identified. More importantly, this work expands our understanding of the consequences of lipid dynamics near the lid margins for tear film formation.

Keywords: tear film, lipid layer, thin film, boundary conditions.

1. Introduction

Each eye blink replenishes the tears on the ocular surface. This deposited tear film left behind after the upstroke is important for vision and ocular health: the tear film protects the eye in a variety of ways beyond just keeping the ocular surface moist (Holly and Lemp, 1977). This multilayer film (Mishima, 1965; Ehlers, 1965) has an anterior layer comprising nonpolar lipids that is tens of nanometers thick and is in contact with air (Norn, 1979; Bron et al., 2004; King-Smith et al., 2009). Polar lipids and other surface active materials are at the interface between this lipid layer and a primarily aqueous layer that is posterior to the lipid layer and is a few microns thick (Holly and Lemp, 1977; King-Smith et al., 2004). The glycogalyx is a mucin-rich region at the aqueous/cornea interface composed primarily of transmembrane mucins that protrude from the epithelial cell membranes (Chen et al., 1997; Gipson, 2004; Govindarajan and Gipson, 2010). The tear film is a few microns thick in the center of the cornea after a blink (King-Smith et al., 2004, 2006; Wang et al., 2003) and it has a considerably thicker meniscus (about 0.065 mm or more) around the lid margins where the tear film climbs the wettable part of the eyelid (Palakuru et al., 2007; Johnson and Murphy, 2006; Harrison et al., 2008). This structure must be re-formed rapidly after blinks to enable vision with minimal interruption.

The lipid layer is supplied from the lid margin, and the lipids wet the lid margin. The idea of a

lipid reservoir at the lids was summarized in the review by Bron et al. (2004) in their Section 7. They discussed a method developed by Chew et al. that estimates the amount of lipid stored at the lid margin (Chew, Hykin, Jansweijer, Dikstein, Tiffany and Bron, 1993; Chew, Jansweijer, Tiffany, Dikstein and Bron, 1993). By applying a tape at the central lower lid margin, they extracted an estimated 60 μg of the lipid; the total amount on the tape was estimated using optical and balance methods. Moreover, they estimated about 300 μg of lipid was stored at a casual or steady state level around the lid margin. They also assumed a typical thickness for the lipid layer covering the tear film and estimated the amount of lipid need to establish this uniform lipid layer of typical thickness to be about 9 μg. This value is similar to an estimate of a uniform lipid layer of 50 nm over 2.9 cm^2 exposed surface area of the cornea (Tiffany, 1991) with an estimated specific gravity of 0.95; with those quantities, one obtains 14 μg of lipid. They concluded the so-called lipid reservoir around the lid margin stored ample amounts of lipid (300 μg compared to 14 μg) to draw from while establishing the lipid layer during blinks.

The quantum dot visualization of Khanal and Millar (2010) also supports the notion of a lipid buildup or reservoir at the lid margin; see their Figure 3. This appears to be anterior to the edge of the mucosal part of the lid margin (the mucocutaneous junction), and it seems plausible that the buildup area of the lid margin ends there. The authors do not clearly establish the location of the end of the buildup however. The buildup area certainly extends beyond the base of the lashes; see their Figure 3F. The "jetting" from the meibomian orifice in their Figure 3C support this notion, since the meibomian orifices are anterior to the mucocutaneous junction but posterior to the base of the lashes. However, Khanal and Millar (2010) show that there is a flux of lipids to and from the lipid reservoir. They find lipophilic quantum dots are spread repeatedly onto the surface of the tear film following blinks and that after some time quantum dots exit the tear film onto the lids and lashes. It is not immediately clear how a steady state reservoir should be treated in a fluid dynamic model. As a first step, we study different boundary conditions (BCs) for treating the lipid concentration at the lid margin; these are discussed further below.

The overall rate of turnover of the lipid layer was estimated by Mochizuki et al. (2009) and they compared it to the aqueous layer turnover rate. They used sodium fluorescein as an aqueous layer tracer, and 5-dodecanoylaminofluorescein (DAF) as a lipid layer tracer (insoluble in aqueous layer). Both tracers fluoresce under appropriate illumination, and can be monitored by an appropriate optical system. By monitoring the decrease in fluorescent intensity of the emissions from the layers, they estimated that the lipid layer turns over a little more than 10 times slower than the aqueous layer. While this result does not give detailed information about what is happening at the lid margin, it does suggest that overall exchange between the lipid layer and the lid is much slower than aqueous supply and drainage. We interpret this to mean that the lipid reservoir is likely an "imperfect" one in that it does not exchange lipid infinitely rapidly between lid and tear. According to a recent review of tear turnover rates (Garaszczuka et al., 2018), there has been one other attempt to measure tear lipid turnover rate. Napoli et al. (2014) used a castor oil suspension, imaged via optical coherence tomography, as a proxy to estimate tear film lipid layer turnover. While interesting imaging of flow in the menisci was reported, the suspension was clearly inside the aqueous layer and so the relationship of the measurement to the insoluble naturally-occurring tear film lipid layer seems unclear at the time of writing.

The term "blink cycle" is used to mean the combined periods of a single blink, in which the upper lid moves down toward the lower lid and returns, together with the interblink period separating two blinks. Depending on whether the upper lid meets the lower lid by the end of the blink cycle, a blink is further characterized as a "full blink" or "partial blink." The blink rate measures the frequency of tear re-distribution and is an indicator of the health and proper function of the eye. The blink rates vary among individuals or for the same individual according to various conditions such as age, ocular surface health or mental focus (Himebaugh et al., 2009; Cruz et al., 2011). Though blink rates can vary between

2-3 blinks/min up to 20-30 blinks/min, a typical blink rate is about 12-20 blinks/min when the subject is at rest under a neutral environment condition (Sibony and Evinger, 1992; Freudenthaler et al., 2003; Tsubota, 1998; Monster et al., 1978). A blink rate of 12 blinks/min gives an average interblink interval of about 5 seconds (assuming there is no mental task requiring concentration). Partial blinks are not uncommon, ranging from 10 to 80% depending on the experimental conditions (Carney and Hill, 1982; Abelson and Holly, 1977; Doane, 1980) and subject health (McMonnies, 2007).

Linked to the blink cycle is the supply and drainage of the tear film. In his theory of the lacrimal system, Doane (1980) posed that significant drainage along the lid margins begins with the lids about halfway open, and that it ends up to 3 seconds after the lids have fully opened. New tear fluid is supplied from the lacrimal gland, which secretes the aqueous part of the tear film, and this new fluid is observed to enter the exposed tear film from the superior lid near the outer (temporal) canthus (Lorber, 2007; Maurice, 1973; Doane, 1980; Harrison et al., 2008). The aqueous part of tears exits via the puncta, which are small drain holes found near the nasal canthus (Oyster, 1999).

A number of studies of the tear film that considered only the interblink found reasonable break-up times (BUT) for the film. They also found the minimum thickness was proportional to $t^{-0.45}$ or $t^{-0.46}$ for long times in the "black line" region (Wong et al., 1996; Sharma et al., 1998; Miller et al., 2002; Braun and Fitt, 2003). This name comes from the experimental observation that thinning is most significant along the line-shaped regions near the lid margins, which appear as dark regions when measured with fluorescence techniques (Miller et al., 2002; Nichols et al., 2012). Building off the successful theoretical studies on interblink period, there is a large body of work studying not only the relaxation of the tear film (dynamics during the interblink), but the formation and re-formation of the tear film during lid motion. These theoretical models of tear film dynamics have recently been reviewed in Braun (2012) and Braun et al. (2015).

In this paper, we simplify the lipid layer to the limiting case of an insoluble surfactant. This simplification was used in Jones et al. (2006) and Aydemir et al. (2010); they used a dilute surfactant model and a relatively thick aqueous layer with large menisci to compute the effects on the aqueous layer and polar lipid distribution. Both papers found similar qualitative behavior to observed tear film thickness distributions, and both papers predicted a decreasing concentration of polar lipids at the lids during the blink. Aydemir et al. (2010) found analytical approximations for the computed dynamics. Allouche et al. (2017) added a spherical substrate to the computations and found minor differences in the minimum thicknesses and polar lipid concentrations. Zubkov et al. (2012) added dynamics for solutes representing osmolarity in the aqueous layer as well as saccadic motion of the ocular surface. The model of Bruna and Breward (2014) included a second nonpolar fluid layer as well as an aqueous layer and an insoluble surfactant. They found complex dynamics for the lipid and aqueous layers, and several limiting cases for simplifying the models. The dynamics for the lipid layers was especially complicated near the moving boundary corresponding to the upper lid, with narrow layers existing in that region.

We revisit the simpler case without the nonpolar lipid layer, and explore the consequences of other choices for the BCs outlined in Section 2. We use mixed BCs on the surfactant, which in limiting cases, may either represent a surfactant reservoir (Chew, Hykin, Jansweijer, Dikstein, Tiffany and Bron, 1993; Chew, Jansweijer, Tiffany, Dikstein and Bron, 1993) or the no flux case (Aydemir et al., 2010). The resulting dynamics capture only some aspects of the tear film as discussed in Section 3, but they do lead to additional understanding of tear film dynamics and how the component parts affect those dynamics summarized in Section 4. We end by summarizing our conclusions in Section 5.

2. Problem Formulation

To study the influence of the lipid reservoir, we consider the tear film dynamics along a line running down the center of eye opening (the palpebral fissure) from the upper lid to the lower lid. The lower lid is fixed at $y' = 0$ and the upper lid moves according to $y' = L'(t')$, where t' denotes time. The ocular surface is assumed to be stationary and flat (Berger and Corrsin, 1974; Braun et al., 2012). Between the lids, we assume the tear film consists of a water layer, $0 \leqslant z' \leqslant h'(y',t')$, to mimic the aqueous layer covered with an insoluble surfactant, whose concentration per unit surface area is given by $\Gamma'(y',t')$, to model the lipid layer.

To understand the influence of the BCs at the lid margins on the dynamics, we study the coupled system previously presented by Aydemir et al. (2010). The mathematical model comprises a thin film equation for $h'(y',t')$, governing the evolution of the aqueous layer thickness, coupled to an advection-diffusion equation for $\Gamma'(y',t')$, governing the movement of the lipid concentration on the moving domain $0 < y' < L'(t')$. We now briefly explain the derivation of the coupled system and then focus our attention on a new set of BCs.

As in Aydemir et al. (2010), the evolution of the aqueous layer is governed by the two-dimensional Navier-Stokes equations, where we denote the velocity of the aqueous fluid in the y'- and z'-directions by $\mathbf{u}' = (v'(y',z',t'),w'(y',z',t'))$, respectively; the pressure by p'; the acceleration due to gravity, which points in the negative y' direction, by g; and the density and viscosity of the aqueous layer by ρ and μ, respectively. At the surface of the eye, $z' = 0$, we assume no slip and impermeability. At the surface of the tear film, $z' = h'(y',t')$, we enforce the kinematic condition; the normal stress balance, where surface tension is denoted by γ; and the tangential stress balance including a surface tension gradient.

The surface concentration of insoluble surfactants on the aqueous/air interface is governed by the advection-diffusion equation for surface transport, where D denotes the surface diffusion coefficient (Stone, 1990). The surfactant transport is coupled with the aqueous layer dynamics through an equation of state for the surface tension. Specifically, as Aydemir et al. (2010), we assume that

$$\gamma = \gamma_0 - RT\Gamma', \tag{2.1}$$

where $R = 8.31$ J/mol K is the universal gas constant, $T = 310$ K is body temperature, and $\gamma_0 = 4.5 \times 10^{-2}$ N/m is the surface tension of the pure aqueous layer (no surfactant present) (Berger and Corrsin, 1974).

The characteristic thickness of the tear film (H) is much smaller than the half-length of the open eye (L_e), $\varepsilon = H/L_e \ll 1$; we may then use lubrication theory to simplify the equations. We nondimensionalize the two-dimensional governing system using the following scales:

$$y = \frac{y'}{L_e}, z = \frac{z'}{H}, h = \frac{h'}{H}, v = \frac{v'}{V}, w = \frac{w'}{\varepsilon V}, t = \frac{t'}{L_e/V}, \Gamma = \frac{\Gamma'}{\Gamma^*}, p = (p' - p'_0)\frac{H^2}{\mu V L_e},$$

where V is average velocity of the lid during the upstroke (opening phase), and Γ^* is a characteristic lipid concentration found by assuming $RT\Gamma'$ in Eqn. (2.1) should be 10^{-3} N/m or smaller (Aydemir et al., 2010). The numerical values of the dimensional parameters are summarized in Table 1.

2.1 *PDEs for h and Γ*

The leading-order equations for the aqueous dynamics can be combined to form a single partial differential equation (PDE) for the evolution of the aqueous layer thickness h in terms of the flux of aqueous

Parameter	Value	Source
H	5×10^{-6} m	(Braun, 2012)
L_e	5×10^{-3} m	(Braun, 2012)
V	4.4×10^{-2} m/s	(Aydemir et al., 2010)
μ	1.3×10^{-3}N.s/m^2	(Jones et al., 2006; Aydemir et al., 2010)
ρ	1.0×10^{3} kg/m^3	(Jones et al., 2006; Aydemir et al., 2010)
γ_0	4.5×10^{-2} N/m	(Jones et al., 2006; Aydemir et al., 2010)
A	3.3×10^{-19} J	(Braun, 2012; Winter et al., 2010)
T	310 K	(Braun, 2012)
Γ^*	4×10^{-7} mol/m^2	(Aydemir et al., 2010)
D	3×10^{-8} m^2/s	(Aydemir et al., 2010)

Table 1. Dimensional parameters.

tears, Q_a:

$$\begin{aligned} \partial_t h + \partial_y Q_a &= 0, \\ \text{where } \; Q_a(y,t) &= -\frac{h^3}{3}\left(\partial_y p + \mathrm{G}\right) - \mathrm{Ma}\frac{h^2}{2}\partial_y \Gamma, \\ \text{and } \; p(y,t) &= -\,\mathrm{S}\partial_y^2 h. \end{aligned} \tag{2.2}$$

(See Aydemir et al. (2010) for a complete derivation.) The nondimensional parameter $\mathrm{G} = \rho g H^2/\mu V$ characterizes the relative importance of gravity and viscosity. $\mathrm{Ma} = \varepsilon RT\Gamma^*/\mu V$ is proportional to the Marangoni number and characterizes the relative importance of surface tension gradients and viscous drag. The nondimensional parameter $\mathrm{S} = \varepsilon^3\gamma_0/\mu V$ is proportional to the inverse capillarity number.

The leading-order equation for the surface concentration of a representative polar lipid is governed by

$$\begin{aligned} \partial_t \Gamma + \partial_y Q_l &= 0, \\ \text{where } \; Q_l(y,t) &= v_s\Gamma - \frac{1}{\mathrm{Pe}}\partial_y\Gamma, \\ \text{and } \; v_s(y,t) &= -\frac{h^2}{2}\left(\partial_y p + \mathrm{G}\right) - \mathrm{Ma}\, h\partial_y\Gamma. \end{aligned} \tag{2.3}$$

The surface flux of lipid is denoted by Q_l and the surface Péclet number is $\mathrm{Pe} = VL_e/D$. In contrast to Aydemir et al. (2010), we retain surface diffusivity as large lipid concentration gradients may form in the lipid reservoir simulations. A summary of the nondimensional parameters is given in Table 2.

Parameter	Expression	Value
ε	$\frac{H}{L_e}$	1×10^{-3}
S	$\frac{\gamma_0\varepsilon^3}{\mu V}$	7.86×10^{-7}
G	$\frac{\rho g H^2}{\mu V}$	4.2×10^{-3}
Pe	$\frac{VL_e}{D}$	7.3×10^{3}
Ma	$\frac{\varepsilon RT\Gamma^*}{\mu V}$	1.8×10^{-2}
$\mathscr{F}$	$V\mathscr{F}'$	$[0,\infty)$

Table 2. Dimensionless parameters. The values of the dimensional parameters are given in Table 1.

2.2 *Boundary Conditions*

In this work, we explore different BCs imposed at the lower and upper lids in order to model a lipid reservoir. Since the evolution equation for the tear film thickness is a fourth-order PDE, we must impose four BCs to uniquely determine a solution. To match what is typically understood to be realistic tear film dynamics, we would like to impose the following three conditions at each lid on the aqueous layer: (A1) pin the tear film thickness to mimic the meniscus; (A2) control the flux of aqueous tears, that is, how much aqueous fluid is entering and/or exiting the exposed ocular surface; and finally, (A3) impose the surface velocity to match the lid speed. By using lubrication theory, we lose a degree of freedom through the depth-wise averaging and therefore we must chose two of the three conditions. Additionally, we must impose one BC at each lid to close the lipid concentration evolution equation. The natural choices for BCs at each lid are (L1) to specify the lipid concentration and (L2) to specify the lipid flux to control how much lipid enters the system. It is important to note that the BCs strongly impact the volume of the aqueous tears and the amount of lipid concentration in the tear film. By manipulating the evolution equations, we find the evolution of the aqueous tear volume is given by

$$\frac{d}{dt}\int_0^{L(t)} h(y,t)\,dy = -Q_a(L(t),t)+Q_a(0,t)+h(L(t),t)\dot{L}(t), \tag{2.4}$$

and the evolution of the amount of lipid is given by

$$\frac{d}{dt}\int_0^{L(t)} \Gamma(y,t)\,dy = -Q_l(L(t),t)+Q_l(0,t)+\Gamma(L(t),t)\dot{L}(t). \tag{2.5}$$

In prior works, Jones et al. (2006) imposed (A1), (A2), and (A3) at the upper lid and (A1), (A2), and (L1) at the lower lid. Because the surface velocity and the flux of the aqueous tears are functions of $\partial_y\Gamma$ and $\partial_y^3 h$, BCs (A1), (A2), and (A3) at the upper lid uniquely close the coupled aqueous tear and lipid concentration system. Jones et al. (2006) analyzed how the BCs could be applied at the moving upper lid dynamics and (A3) was chosen to enforce zero lipid advection when lipid diffusion is neglected.

In Aydemir et al. (2010), BCs (A1), (A2), and (A3) are imposed at both the upper and lower lids. Both works took the perspective that the lipid dynamics will adjust at the lids to achieve a desired tear film dynamics and/or tear film volume conservation. As a consequence, the amount of lipid at the lid margins and the amount of lipid entering and exiting the system is not controlled. In contrast, Deng (2013) enforced BCs (A1), (A2), and (L1). As a result, the surface velocity of the tear film adjusts to the imposed BCs and is not controlled.

Here, we take a different approach from these earlier works; we impose various conditions on the lipid concentration at the boundaries and observe the resulting dynamics. To ensure that the advection of the lipid is correctly captured near the boundaries, we impose BC (A3), that is,

$$v_s(0,t) = 0 \text{ and } v_s(L(t),t) = \dot{L}(t). \tag{2.6}$$

For the lipid concentration, we impose the following mixed BCs combining (L1) and (L2). Presented in dimensional form:

$$\left[\Gamma^* - \Gamma'(0,t')\right] - \mathscr{F}' Q_l'^d(0,t') = 0, \tag{2.7}$$

$$\left[\Gamma^* - \Gamma'(L'(t'),t')\right] + \mathscr{F}' Q_l'^d(L'(t'),t') = 0, \tag{2.8}$$

where $\mathscr{F}'$ is a parameter with dimensions of length per time and used to model an imperfect reservoir, and the dimensional diffusive lipid flux is

$$Q_l'^d(y',t') = -D\partial_{y'}\Gamma'(y',t'). \tag{2.9}$$

Physically, if the lipid concentration at the boundary differs from the lipid reservoir concentration, then there is a flux of lipid onto or out of the exposed ocular surface.

The lipid reservoir concentration, specified by the boundary condition $\Gamma' = \Gamma^*$, is no doubt a simplification of the actual state of the lipid layer at the eyelid margin. The approximation of insolubility is likely a very good assumption (Bron et al., 2004), and we go further to assume that the floating nonpolar layer with an insoluble surfactant at a lipid/aqueous interface can be simplified to an insoluble monolayer in a gaseous state. This has been done previously Aydemir et al. (2010), and it is mathematically tractable. It is certain that when the lids are close together, the surface concentration of the surfactant is high, and all of our computations start at this "closed" state. The Dirichlet boundary value is chosen to match the high value of this closed state and to stay there. It is likely a simplification of the actual level of polar lipid that may be present at the surface in the closed state; the polar lipid may not even be a monolayer when the lids are close together. Incorporating multilayers and the transition to a monolayer is beyond the scope of our models in this paper. In light of that limitation, and the lack of detailed *in vivo* information at the lid margins, this assumption of the constant high value initially is a rational choice.

The nondimensional form of the boundary conditions are given by

$$[1 - \Gamma(0,t)] + \frac{\mathscr{F}' D}{L_e}\partial_y \Gamma|_{y=0} = 0, \tag{2.10}$$

$$[1 - \Gamma(L(t),t)] - \frac{\mathscr{F}' D}{L_e}\partial_y \Gamma|_{y=L(t)} = 0, \tag{2.11}$$

where the parameter $\mathscr{F}'$ is now multiplied by the characteristic surface diffusion speed. We measure $\mathscr{F}'$ relative to the characteristic lid speed to derive the non-dimensional form:

$$[1 - \Gamma(0,t)] + \frac{\mathscr{F}}{\mathrm{Pe}}\partial_y \Gamma|_{y=0} = 0, \tag{2.12}$$

$$[1 - \Gamma(L(t),t)] - \frac{\mathscr{F}}{\mathrm{Pe}}\partial_y \Gamma|_{y=L(t)} = 0. \tag{2.13}$$

We view the mixed lipid boundary condition models as an imperfect reservoir and later we show how the dynamics of the system change when $\mathscr{F} = \mathrm{Pe}$. If the kinetics of letting the lipid out from the reservoir is fast, then $\mathscr{F}$ is small to compared to Pe. If the kinetics of lipid leaving the reservoir are slow, then the lipid concentration at the boundary can change significantly, $\mathscr{F}$ is large compared to Pe, and the derivative of lipid concentration is small at the boundary. The limit of the latter is the case treated by previous models (Jones et al., 2006; Aydemir et al., 2010).

There are two different limiting behaviors. When $\mathscr{F} = 0$, the lipid concentration is fixed via a Dirichlet condition, $\Gamma(0,t) = \Gamma(L(t),t) = 1$, and from Eqn. (2.5), the total amount of lipid on the exposed ocular surface is governed by

$$\frac{d}{dt}\int_0^{L(t)} \Gamma(y,t)\, dy = \frac{1}{\mathrm{Pe}}\partial_y\Gamma(L(t),t) - \frac{1}{\mathrm{Pe}}\partial_y\Gamma(0,t). \tag{2.14}$$

Because we are not specifying lipid concentration gradients at the boundary in this case, the amount of lipid in the domain will likely change with time. In the limit when $\mathscr{F} \to \infty$, homogeneous Neumann conditions are imposed on $\Gamma(y,t)$ at the ends. This case results in

$$Q_l^d(0,t) = 0 \text{ and } Q_l^d(L(t),t) = 0. \tag{2.15}$$

Therefore, in the limit of $\mathscr{F} \to \infty$, combining the surface velocity conditions (2.6) with appropriate no-flux conditions from Eqn. (2.5), the total amount of lipid concentration on the exposed eye will be conserved.

For the final BCs, we pin the tear film thickness, BC (A1),

$$h(0,t) = h_0 \text{ and } h(L(t),t) = h_0, \tag{2.16}$$

to mimic the tear film meniscus. Throughout this work, we assume the tear film thickness at the lid is either 1000 μm ($h_0 = 200$) to compare to prior work of Aydemir et al. (2010) or the more realistic value of 65 μm ($h_0 = 13$) (Palakuru et al., 2007; Johnson and Murphy, 2006; Harrison et al., 2008). We note the lubrication approximation assumption is not satisfied in the menisci regions, but the lubrication approximation has been shown to still make reasonable predictions (Benilov and Zubkov, 2008; Zubkov et al., 2013).

2.3 *Lid motion*

To compare our simulations to the results in Aydemir et al. (2010), we characterize the upper lid motion using their function created from fitting experimental data presented in Wong et al. (1996). Specifically,

$$L(t) = \begin{cases} L_{cl} + U_0\tau\left\{-\frac{1}{2}\left[\frac{t}{\tau}\right]^2 + \lambda\left[\frac{\sqrt{\pi}}{2}\,\mathrm{erf}\left(\sqrt{\frac{t}{\tau}}\right) - \sqrt{\frac{t}{\tau}}\,\mathrm{e}^{-t/\tau}\right]\right\}, & t \leqslant t^* \\ L_{op}, \qquad t > t^* \end{cases} \tag{2.17}$$

with nondimensional parameters $L_{cl} = 0.4$, $U_0 = 0.37$, $\lambda = 11.6$, $\tau = 0.765$, and $t^* = 1.59$. Physically, the lids start at a distance of 0.2 cm apart and then the upper lid moves 0.8 cm over 0.18 seconds to open fully. Figure 1 show the upper lid position and speed.

2.4 *Initial Conditions*

We assume the tear film thickness is initially given by

$$h(y,0) = h_0, \tag{2.18}$$

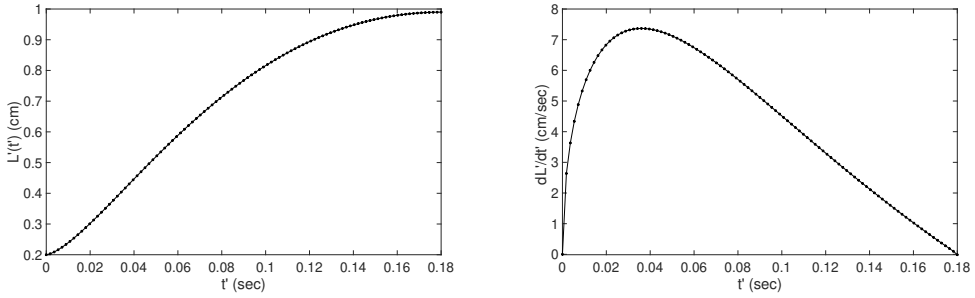

FIG. 1. The motion of upper lid (left) and its speed (right).

where h_0 is the constant specified value at the boundary. The initial polar lipid concentration is uniform with

$$\Gamma(y,0) = 1; \tag{2.19}$$

in that case, the surfactant concentration is the representative value Γ^* uniformly across the initial domain. Varying the initial distribution of Γ while fixing the BCs made little difference in the solution after a very short time. The domain typically begins in the closed state with

$$L(0) = 0.20. \tag{2.20}$$

2.5 *Numerical Method*

We must solve the system of PDEs (2.2) and (2.3) subject to BCs (2.6), (2.12), (2.13), and (2.16) as well as the initial conditions (2.18), (2.19), and (2.20). We first map the moving domain $0 < y < L(t)$ into the fixed domain $0 < s < 1$ via $s = y/L(t)$. Next, the system of evolution equations is approximated on the fixed domain using a method of lines approach. The spatial derivatives are first approximated with second-order centered finite differences on a uniform spatial grid. The resulting system of ordinary differential equations are integrated forward in time in MATLAB using `ode15s`. The typical number of grid points used in the computations is $N = 8191$. To validate our numerical scheme, we have confirmed the volume of the tear film is conserved to second-order accuracy in the spatial grid spacing.

3. Results

In what follows, we conduct a parameter study to explore the consequences of imposing different BCs controlling the lipid dynamics at the lid margins. We focus on exploring how the presence of the lipid reservoir affects the tear film formation during the upstroke. We begin by considering different values of $\mathscr{F}$ both excluding and including the effects of gravity. Dimensionally, the initial tear film thickness is constant at 10^3 μm (nondimensionally, $h_0 = 200$), and the initial lipid concentration is 4×10^{-7} mol/m^2. We note the initial cross-sectional area of the tear film is 0.02 cm^2. To compare to measured tear volumes on the exposed eye, we can multiply this area, 0.02 cm^2 (width x height), by 2.5 cm (an approximate length of the palpebral fissure from nose to temple) to obtain an upper bound of the tear film volume of 50 μl. This volume is twenty times the estimate of the tear film volume of 2.45 μl from Mishima et al. (1966). The initial condition was chosen to compare our findings to Aydemir et al. (2010).

3.1 *Pinned Lipid Concentrations at Boundaries*

Figure 2 shows the evolution of the tear film thickness, the pressure, the lipid concentration, and the surface velocity for $\mathscr{F} = 0$ at 0.01-second increments during the upstroke. The tear film quickly forms a roughly parabolic profile followed by the appearance of two quasi-static menisci with a thin connecting film. This evolution is comparable to the findings of Aydemir et al. (2010), mimicking their early and intermediate stages. The differences in the evolution, compared to prior works (Aydemir et al., 2010; Jones et al., 2005; Wong et al., 1996), are confined to the menisci regions; we now analyze the upper meniscus dynamics to characterize the deposition of the tear film.

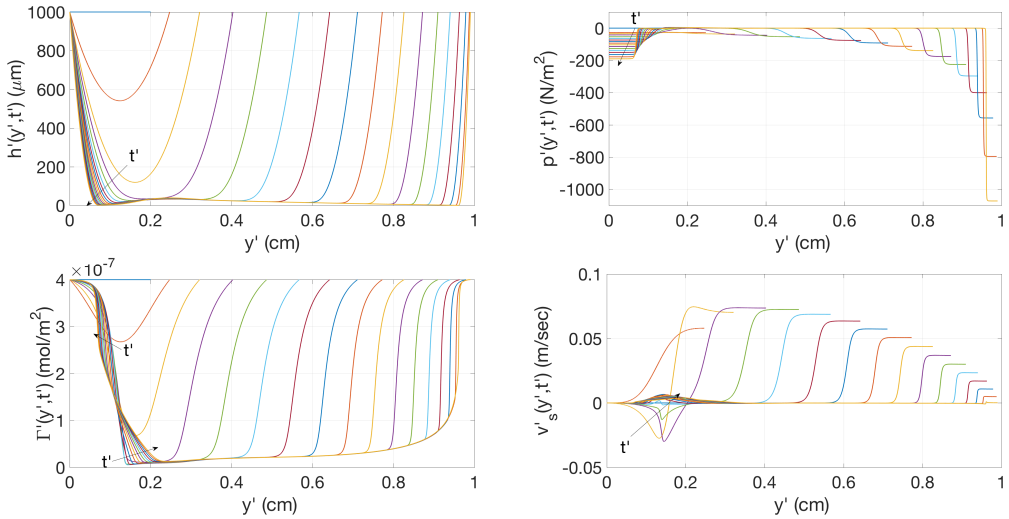

FIG. 2. The upstroke dynamics for the pinned lipid BCs, $\mathscr{F} = 0$, shown at 0.01-second increments. In lexicographic order, the evolution of the dimensional tear film thickness, the pressure, the lipid concentration, and the surface velocity.

3.1.1 *Upper Meniscus* In the upper meniscus, the lipid concentration must adjust to satisfy the specified lipid concentration and lid speed surface velocity BCs. After an initial adjustment, the surface velocity in the upper meniscus, shown in Figure 2, is constant and equal to the lid speed. A similar constant surface velocity interval was observed in Bruna and Breward (2014) in some cases they studied. In general, we find the lipid diffusion to be higher order with $1/\mathrm{Pe} \approx \varepsilon$ (see Table 2), and is negligible for most of the upstroke. Consequently, the lipid concentration in the upper meniscus is advected with the lid speed motion; from Eqn. (2.3), we find $\partial_t \Gamma + \partial_y(\dot{L}\Gamma) = 0$. Locally, the lipid concentration is given by $\Gamma(y,t) = F_l(y - [L(t) - L(t_{v_s})])$, where $F_l(\eta)$ is an arbitrary function determined by the initial conditions. The characteristics are given by $\eta = y - [L(t) - L(t_{v_s})]$, where t_{v_s} is a time after the interval of constant surface velocity has been established in the upper meniscus; they do not intersect.

Turning to the aqueous dynamics, in the upper meniscus, there exists a negative pressure gradient forcing the surface velocity to equal the lid velocity and thus satisfy that BC. Specifically, because the lipid concentration is increasing, the Marangoni stresses result in a flow opposite to the lid motion. This creates the need for a pressure gradient in the upper meniscus to establish the positive surface velocity that is compatible with the lid motion (see Eqn. (2.3)). Consequently, the presence of the lipid reservoir requires larger pressure gradients in the upper meniscus.

Using the known lipid dynamics in the interval of constant surface velocity, we can further characterize the tear film dynamics in the upper meniscus. We can express the pressure gradient in terms of Γ and v_s by rearranging Eqn. (2.3):

$$\partial_y p + \mathrm{G} = -\frac{2v_s}{h^2} - \frac{2\mathrm{Ma}}{h}\partial_y \Gamma. \tag{3.1}$$

Plugging into the expression for the aqueous flux gives

$$Q_a(y,t) = \frac{2h}{3}v_s + \mathrm{Ma}\frac{h^2}{6}\partial_y \Gamma, \tag{3.2}$$

and the evolution of the aqueous thickness is given by

$$\partial_t h + \partial_y \left(\frac{2h}{3}\dot{L} + \mathrm{Ma}\frac{h^2}{6}\partial_y \Gamma \right) = 0, \tag{3.3}$$

where the surface velocity is assumed equal to the lid velocity.

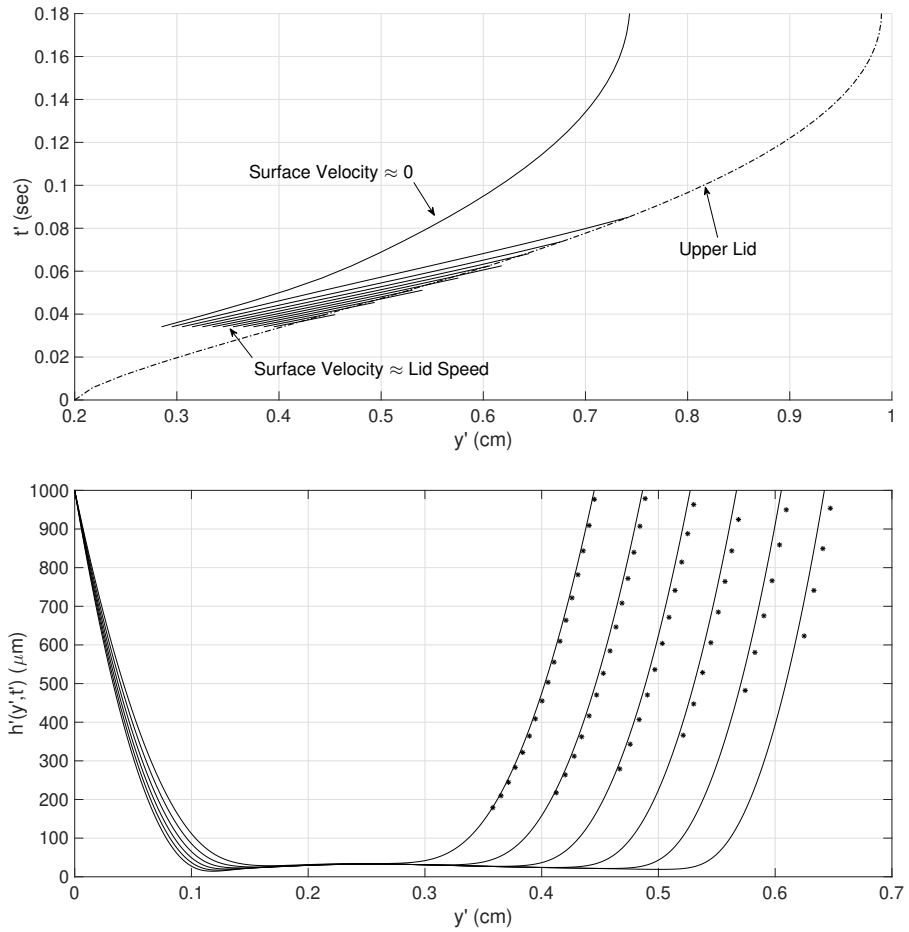

FIG. 3. The top image shows the characteristics for the tear film dynamics in the upper meniscus (solution to Eqn. (3.5)). The bottom image shows the same comparison of the tear film thickness at 0.01-second increments after the constant surface velocity interval is established in the upper meniscus.

To analyze Eqn. (3.3), we apply the method of characteristics:

$$D_t h = -\frac{\mathrm{Ma}}{6} h^2 \partial_y^2 \Gamma \tag{3.4}$$

$$\dot{y} = \frac{2\dot{L}}{3} + \frac{\mathrm{Ma}h}{3}\partial_y \Gamma, \quad y(t_{v_s}) = \eta. \tag{3.5}$$

Here D_t denotes the total derivative along a characteristic, and t_{v_s} is a time after the interval of constant surface velocity has been established in the upper meniscus. The characteristics are determined by Eqn. (3.5) and are plotted in the top image of Figure 3. The characteristics do not intersect and no shocks are present. The characteristics do intersect the curve representing the position of the upper lid. The approximate hyperbolic PDE for the film thickness evolution is not directly using the BC $h(L(t),t) = h_0$. Rather, the tear film and the lipid concentration adjust so that the tear film grows along the characteristic to reach the value of h_0 when its characteristic intersects the upper boundary. The bottom panel in Figure 3 compare the solution of the tear film found by solving the coupled system of partial differential equation (solid lines) to the solution of the approximate hyperbolic partial differential equation for the tear film (dashed lines and * symbols).

The aqueous layer drains significantly in the upper meniscus during the upstroke. With our choice of BCs, we are not conserving the tear film volume because we are not controlling the aqueous flux at the upper lid; the flux is given by

$$Q_a(L(t),t) = \frac{2h_0}{3}\dot{L} + \mathrm{Ma}\frac{h_0^2}{6}\partial_y \Gamma(L(t),t). \tag{3.6}$$

Because both terms are positive, tear fluid is pumped out from the exposed eye at the upper lid. Consequently, when the eye is open, the upper meniscus region only occupies roughly 15% of the exposed eye as opposed to 30% in Aydemir et al. (2010) and the upper meniscus radius decreases during the upstroke. In addition, the tear film ruptures very quickly after the opening (1.88 nondimensional time; in dimensional terms, 0.21 seconds) near the upper lid where the tear film is thinner.

3.1.2 *Deposition Region* The deposition of the tear film is determined by the competition between surface tension gradients (from lipid concentration gradients), which promote tear fluid flow out of the upper meniscus onto the exposed eye, and pressure gradients (from changes in tear/air interface curvature), which promote tear fluid flow into the upper meniscus from the exposed eye. If we express the lipid concentration gradient in terms of the surface velocity and the dynamic pressure gradients (solve for $\partial_y \Gamma$ in Eqn. (2.3)), then we can rewrite the tear film thickness equation as

$$\partial_t h - \partial_y \left[\frac{h^3}{12}(\partial_y p + \mathrm{G}) - \frac{h}{2} v_s \right] = 0. \tag{3.7}$$

Wong et al. (1996) analyzed the same equation but considered the case where the surface velocity was spatially uniform and equal to the lid velocity $v_s(y,t) = \dot{L}(t)$. In the deposition region, Wong et al. (1996) found, through a series of scaling arguments, the tear film dynamics to be quasi-static with capillarity competing with the viscous drag. By matching to a static meniscus with radius R, they found that the thickness of the deposited tear film was given by

$$h_{mid} = 2.1234 R \mathrm{Ca}^{2/3}. \tag{3.8}$$

For comparison, we fit the thickness of the tear film in the middle of the exposed ocular surface at the end of the upstroke for different values of the capillary number $\mathrm{Ca} = \mu V/\gamma_0$ to find $h_{mid} = 246.16\mathrm{Ca}^{0.6112}$. The results are shown in Figure 4. The constant surface velocity confined to the upper meniscus generates similar tear film deposition thicknesses in the middle of the exposed ocular surface.

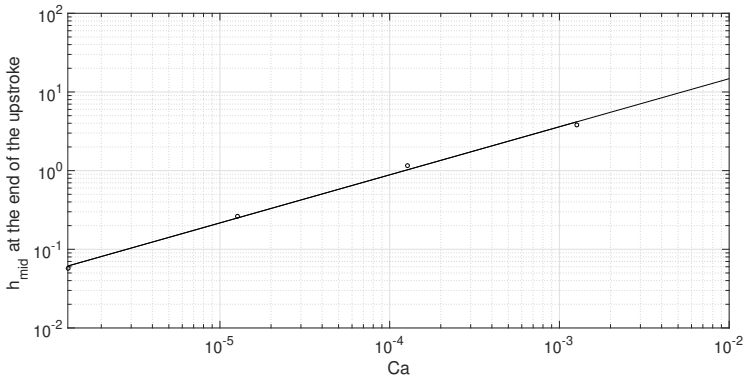

FIG. 4. The tear film thickness in the middle of the exposed ocular surface at the end of the upstroke for different values of the Capillary number, Ca, is plotted as symbols (o). The solid line, given by $h_{mid} = 246.16\mathrm{Ca}^{.6112}$, was found by fitting to the data. The deposited tear film in the center of the eye follows the classic scaling law of capillary number to the two-thirds.

3.1.3 *Lower Meniscus* At the lower lid, the surface velocity is zero and so the lipid flux is determined by diffusion, $Q_l = Q_l^d$. Differentiating the BC, Eqn. (2.12), with respect to time and substituting the result into the evolution equation for Γ, Eqn. (2.3), then near $y = 0$ we find that

$$\mathscr{F}\partial_t Q_l^d - \partial_y Q_l^d = 0. \tag{3.9}$$

Therefore, we have $Q_l^d(y,t) \approx F_l^d(t+\mathscr{F}y)$, where $F_l^d(\eta)$ is an arbitrary function determined by an initial condition. Thus, the lipid diffusive flux is constant along the characteristics defined by $t+\mathscr{F}y = k$, where k is an arbitrary constant. Physically, we can interpret $1/\mathscr{F}$ as a characteristic speed of propagation of the lipid diffusive flux at a stationary boundary. When $\mathscr{F} = 0$, near the lower lid, the lipid concentration is given by $\Gamma(y,t) \approx s_0(t)y+1$, where $s_0(t) < 0$ matches the lipid concentration inside the meniscus (dimensionally, $\Gamma' \approx s_0'(t)y' + \Gamma^*$). We see in the bottom panel of Figure 2 the lipid concentration near the lower lid is linear with the slope approaching zero as time increases (steady-state).

Because the lipid concentration is specified at the lower lid, a lipid concentration gradient is established creating a positive contribution from the Marangoni effect in the lower meniscus. As in the upper meniscus, the pressure-driven flow near the lower lid must counter the established Marangoni flow to satisfy the surface velocity BC at the lower lid:

$$\partial_y p(0,t) + \mathrm{G} = -\frac{2\mathrm{Ma}}{h_0}\partial_y\Gamma(0,t). \tag{3.10}$$

Consequently, we find the aqueous flux at the lower lid, given by

$$Q_a(0,t) = \mathrm{Ma}\frac{h_0^2}{6}\partial_y\Gamma(0,t) = -\mathrm{MaPe}\frac{h_0^2}{6}Q_l^d(0,t), \tag{3.11}$$

is proportional to the diffusive lipid flux. Therefore, the BC for the lipid plays an important role in determining the meniscus dynamics. During the upstroke, the aqueous flux removes tear fluid from the exposed tear film at the lower lid, thus accelerating the tear film thinning in the black line region.

3.1.4 *Effect of Gravity* Including gravitational acceleration only affects the dynamics in the upper and lower menisci. In the upper meniscus, a region of constant surface velocity is established that travels with the lid. Consequentially, capillarity must now compete with both Marangoni and gravitational flows pulling tear fluid out of the upper meniscus onto the exposed eye. Therefore, to satisfy the surface velocity BC, the capillarity needs to be larger resulting in a upper meniscus with more curvature and less tear fluid.

At the lower lid, the gravitational contribution to flow is in the opposite direction of the Marangoni flow. To establish zero surface velocity at the boundary, capillarity cooperates with gravity, which both drive fluid toward the boundary, and they oppose the Marangoni effect, which carries tear fluid out of the lower meniscus and away from the boundary. Consequently, the lower meniscus has less curvature and more tear fluid.

In the center of the exposed tear film, gravitational effects are negligible during the upstroke.

3.2 *Lipid No-Flux BC*

We turn to the other limiting case, where $\mathscr{F} \to \infty$, meaning no lipid concentration can enter or exit onto the exposed tear film from the lipid reservoir. Figure 5 shows the evolution of the dimensional tear film thickness, pressure, lipid concentration, and surface velocity at 0.01-second increments during the upstroke with $\mathscr{F} = 10^6$Pe. Now the early and intermediate stages of the tear film formation are no longer distinguishable. In the early stages (first four curves), the tear film profile is roughly parabolic and then continues to be a parabolic shape during the intermediate stage. Thinning no longer occurs because of the large influxes of aqueous tears onto the exposed ocular surface during the upstroke.

Because the tear film thickness is pinned at h_0 as the upper lid sweeps across the eye, the volume of the tear film increases at rate of $h_0\dot{L}$. Therefore, to conserve volume (assuming no aqueous fluid is entering or exiting at the lower lid, $Q_a(0,t) = 0$), the aqueous fluid flux at the upper lid must be equal to $Q_a(L(t),t) = h_0\dot{L}$ (see Eqn. (2.4)). If $Q_a(L(t),t) < h_0\dot{L}$, then the tear volume will increase during the upstroke; otherwise, the tear volume will decrease. Jones et al. (2005) found if the tear film volume is conserved during the upstroke, then there is not enough aqueous tear fluid on the exposed eye for the upper lid to fully open without the tear film rupturing. They introduced an aqueous flux at the upper lid proportional to the lid velocity. It is interpreted as tear fluid entering the exposed eye from the small gap between the bottom of the upper eyelid and the surface of the eye, $Q_a(L,t) = (h_0 - h_e/2)\dot{L}$. Prior works have approximated the gap to be on the order of a few microns (Aydemir et al., 2010). In this work, the aqueous flux at the upper lid also depends on the gradient of the lipid concentration:

$$Q_a(L(t),t) = \frac{2h_0}{3}\dot{L} + \mathrm{Ma}\frac{h_0^2}{6}\partial_y\Gamma(L(t),t).$$

A small positive lipid concentration gradient is needed to conserve the tear film volume during the upstroke. In the no-flux lipid BC, where $\partial_y\Gamma(L(t),t) \approx 0$, the volume of tear fluid on the exposed ocular surface during the blink is given by $\mathscr{V}(t) = \mathscr{V}(0) + (L(t) - L(0))(h_0/3)$, where $\mathscr{V}(t) = \int_0^{L(t)} h(y,t)\, dy$. Consequently, there is enough tear fluid on the exposed eye for a roughly parabolic tear film shape to persist. Moreover, after the eye opens, there is enough tear fluid on the exposed eye to adjust to a zero-pressure-gradient state (a steady-state of the system). This case shows a substantial difference between

the results for when both aqueous and lipid fluxes are zero at the ends as in Aydemir et al. (2010); significantly more aqueous fluid is present at the end of the upstroke.

In the lipid no-flux BC, the lipid concentration gradient at each lid is zero. As the eye opens, the amount of lipid on the exposed eye is conserved and therefore as the domain expands, the lipid surface concentration decreases. In contrast to the pinned lipid concentration BC ($\mathscr{F} = 0$), there is no Marangoni flow carrying the tear fluid out of the upper meniscus. Therefore, only a relatively small pressure gradient is established across the upper half of the film resulting in a roughly linear surface velocity profile there. Consequently, only the upper half of the exposed eye is stretched uniformly during the upstroke (roughly linear v_s). On the lower half of the exposed eye surface, there is a smaller Marangoni effect (in comparison to the pinned lipid BC) advecting the lipid concentration in the lower meniscus onto the exposed eye surface and causing the lipid concentration in the lower meniscus to decrease during the upstroke. The surface velocity on the lower half of the exposed eye is a small positive value. After the eye opens, the lipid concentration continues to evolve towards a spatially uniform configuration (a steady-state of the system for this large volume without gravity).

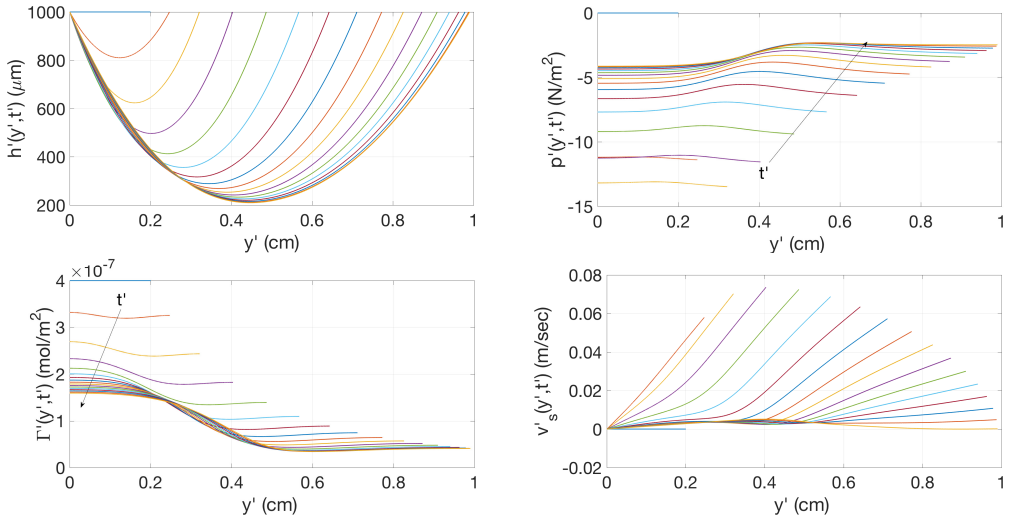

FIG. 5. The upstroke dynamics for the no-flux lipid BCs, $\mathscr{F} = 10^6$Pe, shown at 0.01-second increments. In lexicographic order, the evolution of the dimensional tear film thickness, pressure, lipid concentration, and surface velocity.

3.3 *Mixed Lipid Concentration BC*

We now consider the intermediate case when $\mathscr{F} = \text{Pe}$. In this case, the sizes of gradient of the lipid concentration and the lipid concentration difference at the boundaries are of comparable size.

Figure 6 shows the evolution of the dimensional tear film thickness, pressure, lipid concentration, and surface velocity during the upstroke when $\mathscr{F} = \text{Pe}$. The qualitative behavior of the evolution of tear film thickness and the lipid concentration is similar to the pinned lipid BC, $\mathscr{F} = 0$. The thickness, shown in the top left panel, starts roughly parabolic followed by the configuration of two static menisci connected by a thin film. The thin tear film connecting the two static menisci is concave down. The pressure gradient across the exposed eye works in collaboration with the Marangoni flow to pump tear fluid towards the upper lid.

In comparison with the pinned lipid concentration BCs, there is more aqueous fluid. The aqueous flux of tears at the lids during the upstroke is smaller. The lipid concentration gradient at the lids is smaller than for the pinned lipid concentration BC, but larger than the no-flux lipid BC. Consequently, the meniscus-induced pressure gradients drawing fluid into the meniscus regions are not significantly altered by the required surface velocity BCs. That is, the smaller lipid concentration gradients in the menisci, drawing fluid onto the exposed tear film, result in smaller pressure gradient responses to satisfy the surface velocity BC at the lids (compare magnitude of pressure gradients in Figure 2 to Figure 6). As $\mathscr{F}$ increases and the lipid reservoir becomes less responsive, we find the tear volume increases.

The lipid concentration evolution is shown in the lower left panel of Figure 6. The surface velocity in the upper meniscus, shown in the lower right panel, is no longer constant and equal to the lid speed as with $\mathscr{F} = 0$, nor is it roughly linear as with $\mathscr{F} = 10^6$Pe. In the early stages of the eye opening (first two curves), the surface velocity is roughly linear and the lipid concentration is uniformly stretched across the exposed eye. The advection of the lipid in the upper meniscus cannot maintain the unit lipid concentration. In contrast to the no-flux lipid BC, there is now a dynamic response from the lipid reservoir at the lids. This response is determined by the difference between the actual lipid concentration and unity. Consequently, during the intermediate stages of the upstroke, the surface velocity evolves toward the constant-speed configuration in the upper meniscus observed with $\mathscr{F} = 0$. As the upstroke continues, the lipid concentration at both lids increases as lipid diffuses onto the exposed tear/air interface from the lipid reservoir. Across the exposed tear film, the lipid concentration decreases, and it reaches a minimum in the upper meniscus (similar to the tear film thickness profile with $\mathscr{F} = 0$). At the minimum lipid concentration that forms at later times in the blink, a localized region of strong positive surface velocity forms (Fig. 6, lower right). This pulse of surface velocity continues to propagate up the film faster than the lid near the end of its upward motion and advects polar lipid toward the upper lid. This surface velocity pulse results from the increasing pressure gradient at the end of the lid motion (Fig. 6, upper right), and the lid side of the pulse steepens as it approaches the lid despite the opposing shear stress from the Marangoni effect. In contrast to the pinned lipid concentration case, the lipid concentration appears to drop to zero in our computations and that could be considered breakup of the lipid layer.

3.4 *Smaller Initial Volume*

To make comparisons with other prior studies (Deng et al., 2013, 2014), we consider smaller initial and boundary values for the thickness of $h_0 = 13$ (dimensionally, 65 μm). The initial cross-sectional area is now 1.3×10^{-3} cm^2 and when multiplied by the approximate length of the palpebral fissure, we find an approximate initial tear volume of 2.5 μl. This initial volume is close to the estimate of 2.45 μl for the exposed tear volume from Mishima et al. (1966). Figure 7 shows the evolution of the tear film thickness and the lipid concentration during the upstroke, excluding the effect of gravity, for different values of $\mathscr{F}$. In the pinned lipid concentration BC, $\mathscr{F} = 0$, the tear film ruptures early on during the upstroke at upper lid. The surface velocity advecting the lipid concentration is scaled by the tear film thickness so less aqueous fluid results in smaller surface velocities. The constant surface velocity configuration that travels with the lid velocity cannot be established across the entire upper meniscus region resulting in large lipid concentration gradients. Consequently, at the upper lid, the aqueous flux is large, which starves the upper meniscus.

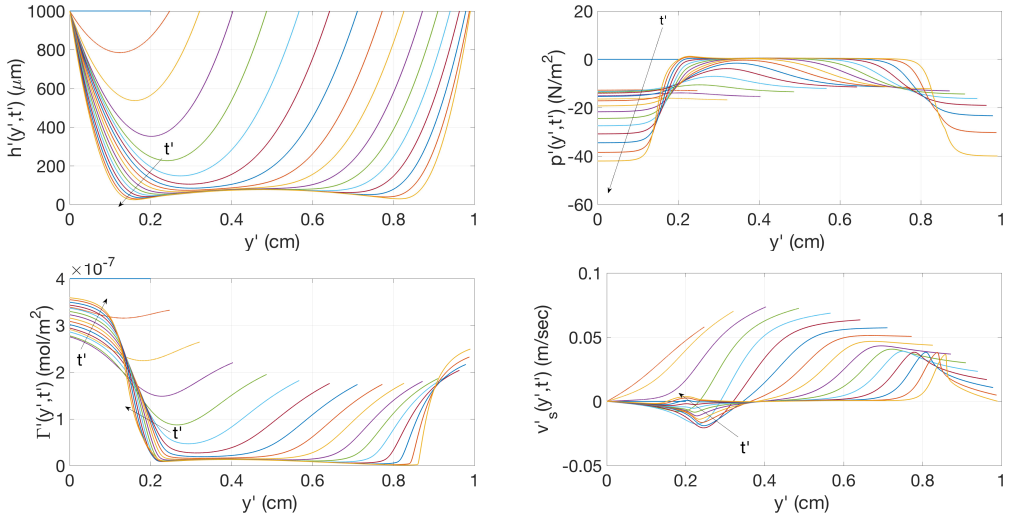

FIG. 6. The upstroke dynamics for the mixed lipid concentration BCs, $\mathscr{F} = \mathrm{Pe}$, shown at 0.01-second increments. In lexicographic order, the evolution of the dimensional tear film thickness, pressure, lipid concentration, and surface velocity.

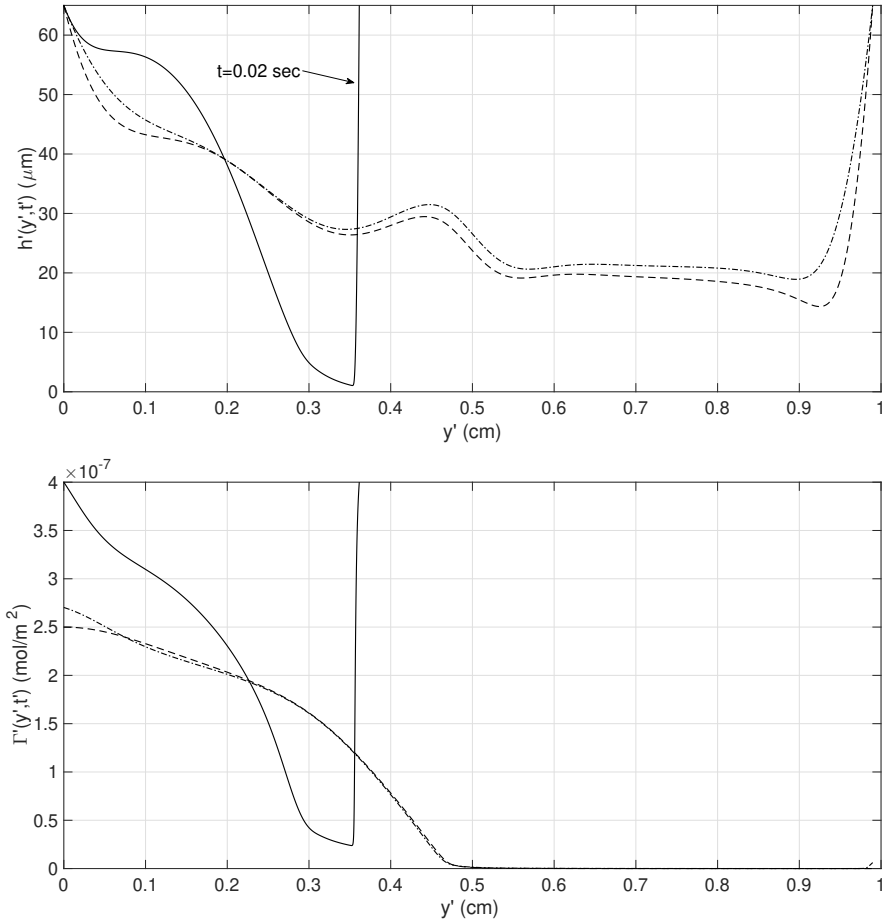

FIG. 7. The tear film thickness and lipid concentration, during the upstroke, at either time of tear film rupture or the end of the upstroke. The pinned lipid BC, $\mathscr{F} = 0$, is the solid line; the mixed lipid BC, $\mathscr{F} = \mathrm{Pe}$, is the dashed-dot line; and the no-flux lipid BC, $\mathscr{F} = 10^6\mathrm{Pe}$, is the dashed line.

As $\mathscr{F}$ increases, the upstroke can be completed without tear film breakup as the smaller lipid concentration gradients in the upper meniscus result in smaller aqueous fluxes at the upper lid. As the lipid reservoir becomes less responsive, the lipid concentration is uniformly stretched across the upper half of the exposed eye resulting in a smaller concentration of lipid close to the upper lid. The dynamics of the mixed and the no-flux lipid BCs become similar as the initial volume of the tear film decreases. To better understand this, Figure 8 shows the evolution of the tear film thickness and lipid concentration during the upstroke for the mixed lipid concentration BC. Specifically, in the bottom right panel, during the intermediate stage of the upstroke, the surface velocity can no longer establish a constant-speed region near the upper lid. Because a constant surface velocity region does not form in the upper meniscus, the dynamics no longer mimic the pinned lipid BC and are now closer to those of the no-flux lipid BCs.

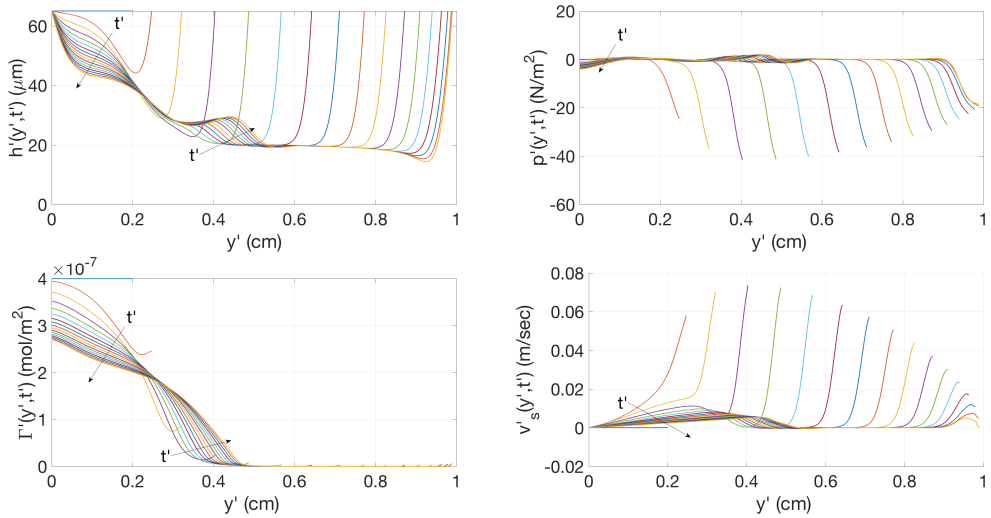

FIG. 8. The upstroke dynamics for the mixed lipid BCs, $\mathscr{F} = \mathrm{Pe}$, shown at 0.01-second increments with the smaller initial tear volume ($h_0 = 13$). In lexicographic order, the evolution of the dimensional tear film thickness, pressure, lipid concentration, and surface velocity.

4. Discussion

In this work, we explore the tear film dynamics when the BCs are chosen to control the lipid dynamics at the lid margins. We assume that at each lid, there exists an imperfect lipid reservoir that attempts to enforce a reservoir lipid concentration at each lid. If the lipid concentration at the lid is less than or more than the reservoir lipid concentration, then onto or out of the exposed tear film. The responsiveness of the lipid reservoir is determined by the size of the parameter $\mathscr{F}$. We study three regimes: (i) $\mathscr{F} = 0$, the lipid concentration is fixed mimicking an instantaneously responsive lipid reservoir; (ii) $\mathscr{F} = \mathrm{Pe}$, the lipid concentration is increased or decreased by diffusing lipid concentration onto or out of from the exposed tear film; and (iii) $\mathscr{F} = 10^6\mathrm{Pe}$, where the lipid reservoir is effectively closed off and the total amount of lipid concentration on the exposed tear film is conserved.

In general, the lipid concentration BC at the lids determines the magnitude of lipid concentration gradients and therefore the size of the Marangoni flow in the menisci regions. Figure 9 displays the influence of parameter $\mathscr{F}$ on the lipid concentration and the size of lipid concentration gradient at

the upper lid over the duration of the upstroke. As $\mathscr{F}$ increases and lipid reservoir responsiveness decreases, the lipid concentration at the upper lid at a given time decreases. Moreover, as $\mathscr{F}$ increases, the amount of time it takes lipid reservoir to reach unity increases. Compare the curves when $\mathscr{F} = 10^3$, $\mathscr{F} = 10^4$, and $\mathscr{F} = 10^5$ in the top plot of Figure 9. In $\mathscr{F} = 10^3$, the lipid concentration reaches unity by the end of the upstroke. When $\mathscr{F} = 10^4$ however, the lipid reservoir is responsive, but the lipid concentration only begins increasing half-way through the upstroke. And when $\mathscr{F} = 10^5$, there is no longer a local minimum in the lipid concentration over the duration of the upstroke. The size of the lipid concentration gradient, and thus the Marangoni contribution to the flow, at the upper lid during the upstroke, is shown in the bottom plot of Figure 9 for different values of $\mathscr{F}$. When the lipid reservoir is responsive ($\mathscr{F}$=0), the size of the Marangoni effect is qualitatively similar to the upper lid speed (compare Figure 1 and Figure 9) where the maximum occurs around 0.04 seconds followed by a linear decrease. As $\mathscr{F}$ increases, the local maximum of the lipid concentration gradients occurs later in the upstroke, eventually disappearing for large enough $\mathscr{F}$. With large $\mathscr{F}$, there are relatively weak Marangoni and capillarity-driven pressure gradient contributions to the flow, and the aqueous layer thickness does not form a localized meniscus near the moving end (e.g., Fig. 7).

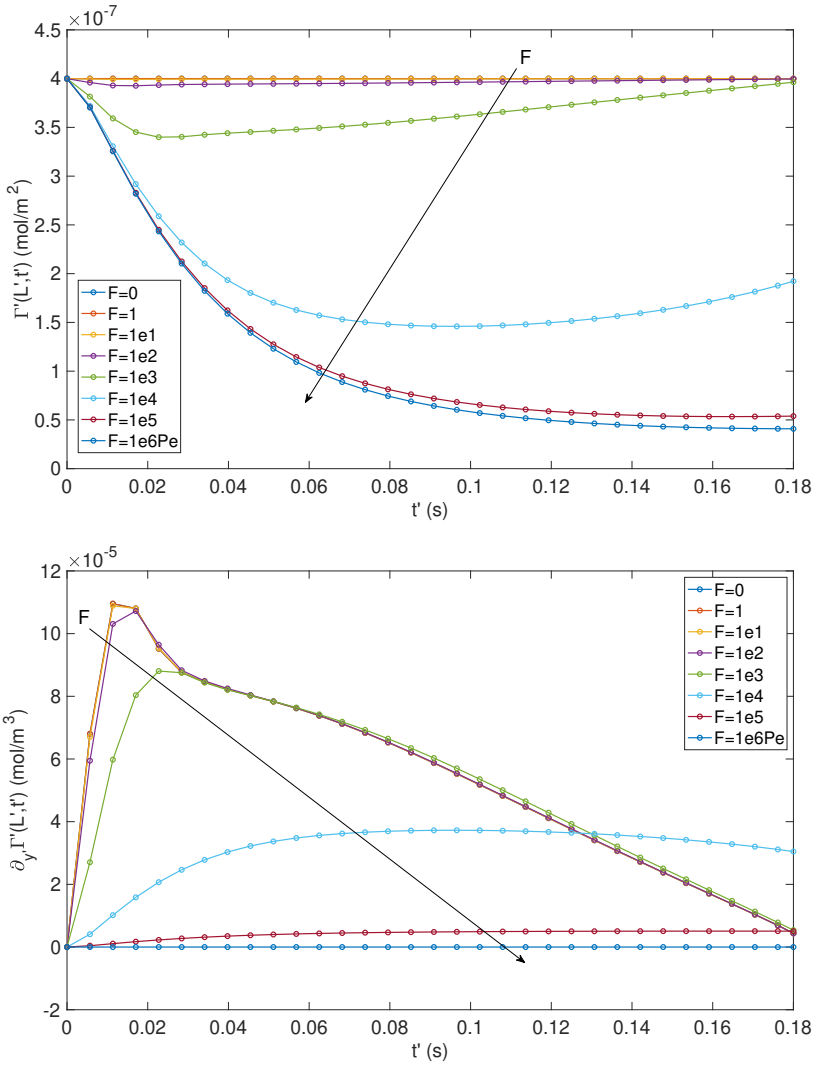

FIG. 9. Boundary values of lipid concentration (top) and the derivative of the lipid concentration (bottom) at the upper lid during the upstroke for different values of $\mathscr{F}$ ranging between 0 and 10^6Pe.

A consequence of the lipid-oriented BCs is that the aqueous flux at the lids is no longer controlled. As the lipid reservoir becomes more responsive, as $\mathscr{F}$ decreases, the lipid concentration gradients at the lids increase. The tear film must respond by establishing an appropriate pressure gradient to satisfy the surface velocity BCs. In the surface velocity equation, the pressure gradient term is scaled by h^2, whereas the lipid concentration gradient term is scaled by h (see Eqn. (2.3)) resulting in a pressure gradient response that is an order of magnitude smaller where the tear film is thin. With the lipid concentration gradient and the pressure gradient set at the lids, the aqueous flux is determined. Specifically, when the lid is not moving, the aqueous flux is proportional to the lipid concentration gradient at the lids. On the other hand, when the upper lid is moving, the tendency of the positive lipid concentration gradient to draw fluid toward the black line is overwhelmed by capillarity in the meniscus which causes significant aqueous outflow at the boundary. The net effect is accelerated thinning in the black line region. In summary, in this model, the lid motion together with the lipid concentration gradients indirectly determine the flux of aqueous fluid at the lids. *In vivo*, the lacrimal gland is the primary source of fresh aqueous fluid, and it receives input from parasympathetic fibers that originate in the pterygopalatine ganglion (Oyster (1999), Ch. 7). The nervous system thus helps determine the influx of new tear fluid (Dartt, 2009). In addition, mathematical tear film models suggest that an appropriate input of aqueous fluid during the upstroke appears to be necessary to form a desirable thickness distribution (Jones et al., 2005, 2006; Aydemir et al., 2010; Bruna and Breward, 2014). Though these latter papers correctly describe aspects of tear film deposition, the nature of the cooperation between the lipid and aqueous inputs to the tear film is still not fully understood.

During the upstroke, the tear/air interface expands as the upper lid moves across the eye. As the lipid reservoir becomes more responsive (i.e., as $\mathscr{F}$ decreases), the surface velocity tends to a constant value equal to the lid speed over a finite interval in the upper meniscus. Consequently, the lipid concentration dynamics near the upper lid change from being uniformly lowered (for larger $\mathscr{F}$) to being advected at the lid speed ($\mathscr{F}$ close to zero). Exploiting the constant surface velocity near the moving lid, we found that the concavity of the lipid concentration determines the growth of the tear film thickness in the upper meniscus. Additionally, with the establishment of the constant surface velocity in the upper meniscus, we found an analogy to the drag-out problem (Park, 1991; Wong et al., 1996). Specifically, during the upstroke, the deposited central tear film thickness is proportional to the capillary number to the two-thirds; the thickness scaling is that same as that found in Wong et al. (1996), though our result is from a different limit. Our responsive lipid reservoir results, $\mathscr{F} < \mathrm{Pe}$, has similar qualitative features to the work of Bruna and Breward (2014). They modeled both the non-polar and polar aspects of the lipid layer. The non-polar lipid layer is modeled as a separate viscous, extensional layer and as done here the polar lipids are described as a surface concentration on the aqueous/non-polar lipid interface. The affect of the extensional non-polar lipid layer on the dynamics of the polar lipid concentration and the surface velocity is similar to a responsive lipid reservoir (compare Figure 3 in Bruna and Breward (2014) to our Figure 6). The extensional velocity, u_2, is qualitatively similar to our surface velocity, v_s, and in both papers these variables can develop localized pulses directed at the boundary. The lipid concentrations have similar profiles in both works as well.

The emergence of the constant speed surface velocity in the upper meniscus can be understood by considering the evolution of the energy associated with evolution of the lipid concentration, Γ. If we multiply Eqn. (2.3) by Γ, integrate by parts, and apply the BCs, then the time rate of change of the

L^2-norm of Γ is given by

$$\begin{aligned}\partial_t\left(\int_0^{L(t)}\frac{1}{2}\Gamma^2\,dy\right) &= -\frac{1}{\mathrm{Pe}}\left\{\frac{\mathscr{F}}{\mathrm{Pe}}\left[\partial_y\Gamma(L(t),t)\right]^2-\partial_y\Gamma(L(t),t)\right\}\\ &\quad -\frac{1}{\mathrm{Pe}}\left\{\frac{\mathscr{F}}{\mathrm{Pe}}\left[\partial_y\Gamma(0,t)\right]^2+\partial_y\Gamma(0,t)\right\}\\ &\quad -\frac{1}{\mathrm{Pe}}\int_0^{L(t)}(\partial_y\Gamma)^2\,dy-\frac{1}{2}\int_0^{L(t)}\Gamma^2\partial_y v_s\,dy. \qquad (4.1)\end{aligned}$$

When $\mathscr{F}<\mathrm{Pe}$ and $\mathrm{Pe}\approx\varepsilon^{-1}$, then the evolution of the system energy is determined by the last integral, a weighted average of the square of the lipid concentration. The weight is given by the extension of the surface. When Γ is closer unit lipid concentration, then the system evolves to a state where $\partial_y v_s\approx 0$. For example, when $\mathscr{F}=0$, the surface velocity is constant and equal to the lid speed in the upper meniscus (see Figure 2). When $\mathscr{F}\approx\mathrm{Pe}$ or larger, the system is more dissipative. The diffusion of lipid near the boundary is too rapid to allow hyperbolic behavior as in the pinned lipid case ($\mathscr{F}=0$).

The initial volume plays a significant role in the ability of the tear film to adjust and establish the constant surface velocity region in the upper meniscus. We have found that as the initial tear film volume decreases, the length of the constant surface velocity region in the upper meniscus decreases. If the lipid concentration is pinned at the ends ($\mathscr{F}=0$), then the tear film breaks up during the upstroke if the initial tear film volume is too small (see Figure 7). Figure 10 summarizes whether or not the tear film can sufficiently coat the substrate (ocular surface) for different values of boundary thickness h_0 and $\mathscr{F}$. We find, for h_0 less than a critical value of $h_0\approx 720\mu$m, that if $\mathscr{F}\geqslant\mathrm{Pe}$, then tear film completely covers the substrate at the end of the upstroke (filled-in symbols). When $\mathscr{F}\leqslant 0.1\mathrm{Pe}$, tear break-up (TBU) occurs before the upstroke ends, and the coating process fails (open circles). The thickness of the established tear film for sufficiently large $\mathscr{F}$ increases significantly for increasing h_0. Figure 10 delineates between minimum tear film thickness greater than 25% of h_0 (filled-in squares) and a minimum thickness less than 25% of h_0 (filled-in circles) When $\mathscr{F}$ is very large, the lipid dynamics mimic the no-flux lipid BC (see Figure 8). When $h_0\approx 720\mu$m or larger, the upstroke is completed and the tear film is established for any of the values of $\mathscr{F}$ that we tested. This critical value of the h_0 is close to the value of 1 mm used in Aydemir et al. (2010).

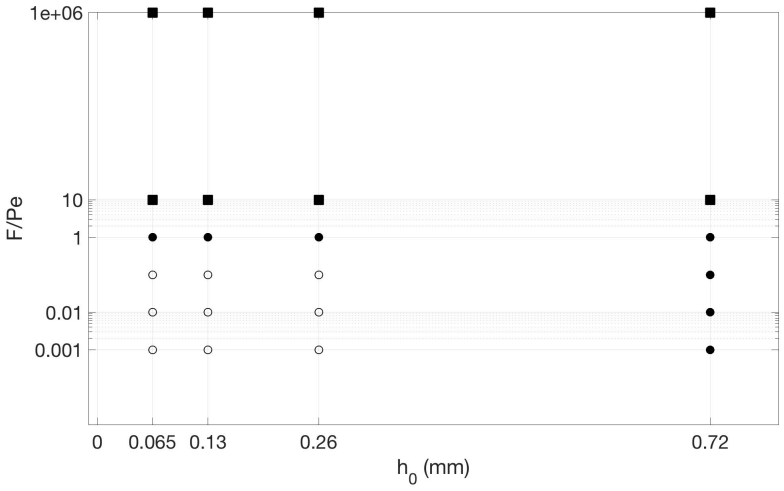

FIG. 10. For given h_0 and $\mathscr{F}$, either (i) the upstroke completes and a minimum film thickness is given (filled-in symbols), or (ii) the tear thickness drops to zero during the upstroke (open circle). The closed circles indicates the minimum tear film thickness is less than 25% of h_0, and the filled in squares indicate minimum tear film thickness is greater than 25%. Above a critical value $h_0 \approx 720\mu$m, the tear film is established at the end of the upstroke for any value of $\mathscr{F}$ that we tested. For smaller h_0, $\mathscr{F} \approx$ Pe or larger enables the upstroke to reach its end with a nonzero thickness throughout the domain.

The model captures some aspects of *in vivo* experiments but not others. For larger $\mathscr{F}$ with thicker films, the lipid concentration dynamics are similar to those in previous models (Aydemir et al., 2010; Bruna and Breward, 2014). In those models, the lipid concentration is lowered in the upper part of the exposed surface at the end of the blink, and motion toward the upper lid will continue after the upstroke. The upward motion of the tear film after the upstroke has been observed experimentally (Berger and Corrsin, 1974; Owens and Phillips, 2001; Jones et al., 2006; King-Smith et al., 2008). Thick regions of lipid can be left behind during the upstroke in some cases (Braun et al., 2015); this may contribute to surfactant concentration gradients that drive the upward motion. As $\mathscr{F}$ decreases and the lipid responsiveness increases, the lipid dynamics become confined to the menisci resulting in smaller changes in the lipid concentration across the exposed eye and thus minimizing any upward Marangoni flow. This is opposed what has been seen experimentally. The lipid concentration in the upper meniscus varies significantly in the pinned lipid BCs, and this is similar to the work of Bruna and Breward (2014). It is typically difficult to capture the dynamics near the lids experimentally as the eyelashes often get in the way, and comparison between theory and experiment is difficult there (Jones et al., 2006; Cruz et al., 2011). Furthermore, direct imaging of surfactant distribution in a spreading film is difficult even in controlled conditions (Sinclair et al., 2018). To our knowledge, direct observation is not available at this time for comparison with the theory.

When controlling the lipid concentration at the boundary and using more realistic tear volumes and thicknesses from recent experiments (King-Smith et al., 2004), the responsiveness of the lipid reservoir $\mathscr{F}$ helps determine whether the upstroke was completed without tear break up. Our lipid BCs, together with the lubrication limit, do not control the amount of aqueous fluid entering or exiting the exposed tear film from under the lids (Jones et al., 2005, 2006; Aydemir et al., 2010) and this may lead to tear break up. In addition, the no-flux lipid BCs as we implemented them could allow for significant influx of aqueous fluid into the tear film that appears to be more than that observed *in vivo*. These aspects suggest the limitations in the model.

5. Conclusions

While there is evidence in the ocular surface literature that there is a lipid reservoir at the lid margins (Chew, Hykin, Jansweijer, Dikstein, Tiffany and Bron, 1993; Chew, Jansweijer, Tiffany, Dikstein and Bron, 1993), there is also visual evidence that a substantial amount of lipid left behind from the upper lid during the upstroke Braun et al. (2015). The reality of how much lipid remains at the lid margin is not clear from experimental work. The model we studied here found a transition in the tear film formation dynamics between cases where the lipid was forced to remain at a high concentration at the lid and when the lipid concentration could vary as in a lipid no flux condition. We also found that a sufficiently large boundary thickness could overcome the transition and allow the tear film to form from a completed upstroke regardless of the lipid condition at the lid. Our results reproduced some results from more complex tear film models (Bruna and Breward, 2014), suggesting that transport of surface active lipids (and perhaps other molecules (Georgiev, 2015)) may sometimes dominate the process of depositing the tear film during the upstroke.

Further work is needed to identify a robust model that incorporates the various aspects of the tear film lipid layer near the lids. The work presented here focused on capturing the lipid dynamics near the lid margins and it highlights some weaknesses of the lubrication theory limit when trying to capture the lipid dynamics and their effect on tear film formation. Approaches along the lines of Zubkov et al. (2013), Khanal and Millar (2010), Mochizuki et al. (2009) and Napoli et al. (2014) may be productive to capture more details of the dynamics near the lids. *In vivo* observations from subjects with lashes

temporarily removed (Jones et al., 2005, 2006) may also yield direct observation of lipid dynamics near the lids using high speed visualization systems (Braun et al., 2015).

6. Acknowledgements

This material is based upon work supported by the National Science Foundation under Grant Numbers DMS 1412141 and 1412085. We thank Prof. David Ross for fruitful discussions.

References

Abelson, M. B. and Holly, F. J. (1977), 'A tentative mechanism for inferior punctate keratopathy', *Am. J. Ophthalmol.* **83**, 866–869.

Allouche, M., Abderrahmane, H. A., Djouadi, S. M. and Mansouri, K. (2017), 'Influence of curvature on tear film dynamics', *Euro. J. Mech. B Fluids* **66**, 81–91.

Aydemir, E., Breward, C. J. W. and Witelski, T. P. (2010), 'The effect of polar lipids on tear film dynamics', *Bull. Math. Biol.* **73**, 1171–1201.

Benilov, E. and Zubkov, V. (2008), 'On the drag-out problem in liquid film theory', *J. Fluid Mechanics* **617**, 283–299.

Berger, R. E. and Corrsin, S. (1974), 'A surface tension gradient mechanism for driving the pre-corneal tear film after a blink', *J. Biomech.* **7**, 225–238.

Braun, R. J. (2012), 'Dynamics of the tear film', *Annu. Rev. Fluid Mech.* **44**, 267–297.

Braun, R. J. and Fitt, A. D. (2003), 'Modeling the drainage of the precorneal tear film after a blink', *Math. Med. Biol.* **20**, 1–28.

Braun, R. J., Usha, R., McFadden, G. B., Driscoll, T. A., Cook, L. P. and King-Smith, P. E. (2012), 'Thin film dynamics on a prolate spheroid with application to the cornea', *J. Eng. Math.* **73**, 121–138.

Braun, R., King-Smith, P., Begley, C., Li, L. and Gewecke, N. (2015), 'Dynamics and function of the tear film in relation to the blink cycle', *Prog. Ret. Eye Res.* **45**, 132 – 164.

Bron, A. J., Tiffany, J. M., Gouveia, S. M., Yokoi, N. and Voon, L. W. (2004), 'Functional aspects of the tear film lipid layer', *Exp. Eye Res.* **78**, 347–360.

Bruna, M. and Breward, C. (2014), 'The influence of non-polar lipids on tear film dynamics', *J. Fluid Mech.* **746**, 565–605.

Carney, L. G. and Hill, R. M. (1982), 'The nature of normal blinking patterns', *Acta Ophthalmol.* **60**, 427–433.

Chen, H.-B., Yamabayashi, S., Ou, B., Tanaka, Y. and Ohno, S. (1997), 'Structure and composition of rat precorneal tear film: A study by *in vivo* cryofixation', *Invest. Ophthalmol. Vis. Sci.* **38**, 381–387.

Chew, C. K. S., Hykin, P. G., Jansweijer, C., Dikstein, S., Tiffany, J. M. and Bron, A. J. (1993), 'The casual level of meibomian lipids in humans', *Curr. Eye Res.* **12**(3), 255–259.

Chew, C. K. S., Jansweijer, C., Tiffany, J. M., Dikstein, S. and Bron, A. J. (1993), 'An instrument for quantifying meibomian lipid on the lid margin: the meibometer', *Curr. Eye Res.* **12**(3), 247–254.

Cruz, A. A. V., Garcia, D. M., Pinto, C. T. and Cechetti, S. P. (2011), 'Spontaneous eyeblink activity', *Ocul. Surf.* **9**, 29–30.

Dartt, D. A. (2009), 'Neural regulation of lacrimal gland secretory processes: Relevance in dry eye diseases', *Prog. Ret. Eye Res.* **28**, 155—-177.

Deng, Q. (2013), Tear Film Modeling in 1D and 2D Moving Geometry with High-Order Methods, PhD thesis, University of Delaware.

Deng, Q., Braun, R. J. and Driscoll, T. A. (2014), 'Heat transfer and tear film dynamics over multiple blink cycles', *Phys. Fluids* **26**, 071901.

Deng, Q., Braun, R. J., Driscoll, T. A. and King-Smith, P. E. (2013), 'A model for the tear film and ocular surface temperature for partial blinks', *Interfacial Phen. Ht Trans.* **1**(4), 357–381.

Doane, M. G. (1980), 'Interactions of eyelids and tears in corneal wetting and the dynamics of the normal human eyeblink', *Am. J. Ophthalmol.* **89**, 507–516.

Ehlers, N. (1965), 'The precorneal film: Biomicroscopical, histological and chemical investigations', *Acta Ophthalmol. Suppl.* **81**, 3–135.

Freudenthaler, N., Neuf, H. and Kadner, G. (2003), 'Characteristics of spontaneous eyeblink activity during video display termnial use in healthy volunteers', *Graefes Arch. Clin. Exp. Ophthalmol.* **241**, 914–920.

Garaszczuka, I. K., Mico, R. M., Iskander, D. R. and Expósito, A. C. (2018), 'The tear turnover and tear clearance tests – a review', *Expert Rev. Med. Dev.* **15**, 219–229.

Georgiev, G. A. (2015), 'Controversies regarding the role of polar lipids in human and animal tear film lipid layer', *Ocul. Surf.* **13**, 176–178.

Gipson, I. K. (2004), 'Distribution of mucins at the ocular surface', *Exp. Eye Res.* **78**, 379–388.

Govindarajan, B. and Gipson, I. K. (2010), 'Membrane-tethered mucins have multiple functions on the ocular surface', *Exp. Eye Res.* **90**, 655–663.

Harrison, W. W., Begley, C. G., Lui, H., Chen, M., Garcia, M. and Smith, J. A. (2008), 'Menisci and fullness of the blink in dry eye', *Optom. Vis. Sci.* **85**, 706–714.

Himebaugh, N. L., Begley, C. G., Bradley, A. and Wilkinson, J. A. (2009), 'Blinking and tear break-up during four visual tasks', *Optom. Vis. Sci.* **86**, E106–E114.

Holly, F. J. and Lemp, M. A. (1977), 'Tear physiology and dry eyes', *Rev. Surv. Ophthalmol.* **22**, 69–87.

Johnson, M. E. and Murphy, P. J. (2006), 'Temporal changes in the tear menisci following a blink', *Exp. Eye Res.* **83**, 517–525.

Jones, M. B., McElwain, D. L. S., Fulford, G. R., Collins, M. J. and Roberts, A. P. (2006), 'The effect of the lipid layer on tear film behavior', *Bull. Math. Biol.* **68**, 1355–1381.

Jones, M. B., Please, C. P., McElwain, D. L. S., Fulford, G. R., Roberts, A. P. and Collins, M. J. (2005), 'Dynamics of tear film deposition and drainage', *Math. Med. Biol.* **22**, 265–288.

Khanal, S. and Millar, T. J. (2010), 'Nanoscale phase dynamics of the normal tear film', *Nanomedicine: Nanotechnology, Biology and Medicine* **6**(6), 707 – 713.

King-Smith, P. E., Fink, B. A., Hill, R. M., Koelling, K. W. and Tiffany, J. M. (2004), 'The thickness of the tear film', *Curr. Eye Res.* **29**, 357–368.

King-Smith, P. E., Fink, B. A., Nichols, J. J., Nichols, K. K., Braun, R. J. and McFadden, G. B. (2009), 'The contribution of lipid layer movement to tear film thinning and breakup', *Invest. Ophthalmol. Vis. Sci.* **50**, 2747–2756.

King-Smith, P. E., Fink, B. A., Nichols, J. J., Nichols, K. K. and Hill, R. M. (2006), 'Interferometric imaging of the full thickness of the precorneal tear film', *J. Optical Soc. Am.* **23**, 2097–2104.

King-Smith, P. E., Nichols, J. J., Nichols, K. K., Fink, B. A. and Braun, R. J. (2008), 'Contributions of evaporation and other mechanisms to tear film thinning and break-up', *Optom. Vis. Sci.* **85**(8), 623–630.

Lorber, M. (2007), 'Gross characteristics of normal human lacrimal glands', *Ocul. Surf.* **5**, 13–22.

Maurice, D. M. (1973), 'The dynamics and drainage of tears', *Int. Ophthalmol. Clin.* **13**, 103–116.

McMonnies, C. W. (2007), 'Incomplete blinking: Exposure keratopathy, lid wiper epitheliopathy, dry eye, refractive surgery, and dry contact lenses', *Cont. Lens Anterior Eye* **30**, 37–51.

Miller, K. L., Polse, K. A. and Radke, C. J. (2002), 'Black line formation and the "perched" human tear film', *Curr. Eye Res.* **25**, 155–162.

Mishima, S. (1965), 'Some physiological aspects of the precorneal tear film', *Arch. Ophthalmol.* **73**, 233–241.

Mishima, S., Gasset, A., Klyce, S. D. and Baum, J. L. (1966), 'Determination of tear volume and tear flow', *Ophthalmol. Vis. Sci.* **5**, 264–276.

Mochizuki, H., Yamada, M., Hatou, S. and Tsubota, K. (2009), 'Turnover rate of tear-film lipid layer determined by fluorophotometry', *Br. J. Ophthalmol.* **93**, 1535–1538.

Monster, A. W., Chan, H. C. and O'Connor, D. (1978), 'Long-term trends in human eye blink rate', *Biotele. Patient Monitor.* **5**, 206–222.

Napoli, P., Coronella, F., Satta, G. M. and Fossarello, M. (2014), 'A novel technique of contrast-enhanced optical coherence tomography imaging in evaluation of clearance of lipids in human tears', *PLOS One* **9**(11), e109843.

Nichols, J. J., King-Smith, P. E., Hinel, E. A., Thangavelu, M. and Nichols, K. K. (2012), 'The use of fluorescent quenching in studying the contribution of evaporation to tear thinning', *Invest. Ophthal. Vis. Sci.* **53**(9), 5426–5432.

Norn, M. S. (1979), 'Semiquantitative interference study of fatty layer of precorneal film', *Acta Ophthalmol.* **57**, 766–774.

Owens, H. and Phillips, J. (2001), 'Spread of the tears after a blink: Velocity and stabilization time in healthy eyes', *Cornea* **20**, 484–487.

Oyster, C. (1999), *The Human Eye – Structure and Function*, Sinauer, Sunderland, MA.

Palakuru, J. R., Wang, J. and Aquavella, J. V. (2007), 'Effect of blinking on tear dynamics', *Invest. Ophthalmol. Vis. Sci.* **48**, 3032–3037.

Park, C. W. (1991), 'Effects of insoluble surfactants on dip coating', *J. Coll. Interface Sci.* **146**, 382–394.

Sharma, A., Tiwari, S., Khanna, R. and Tiffany, J. M. (1998), Hydrodynamics of meniscus-induced thinning of the tear film, *in* 'Lacrimal Gland, Tear Film, and Dry Eye Syndromes 2', Springer, pp. 425–431.

Sibony, P. A. and Evinger, C. (1992), Anatomy and physiology of normal and abnormal eyelid position and movement, *in* N. Miller, ed., 'Walsh & Hoyt's Clinical Neuro-ophthalmology', Baltimore, Williams and Wilkins, pp. 1509–1592.

Sinclair, D., Levy, R. and Daniels, K. E. (2018), 'Simulating surfactant spreading: Influence of a physically motivated equation of state', *Euro. J. Appl. Math.* **29**, 30–54.

Stone, H. (1990), 'A simple derivation of the time-dependent convective-diffusion equation for surfactant transport along a deforming interface', *Phys. Fluids A* **2**(1), 111–112.

Tiffany, J. M. (1991), 'The viscosity of human tears', *Intl. Ophthalmol.* **15**, 371–376.

Tsubota, K. (1998), 'Tear dynamics and dry eye', *Prog. Retin. Eye Res.* **17**, 565–596.

Wang, J., Fonn, D., Simpson, T. L. and Jones, L. (2003), 'Precorneal and pre- and postlens tear film thickness measured indirectly with optical coherence tomography', *Invest. Ophthalmol. Vis. Sci.* **44**, 2524–2528.

Winter, K. N., Anderson, D. M. and Braun, R. J. (2010), 'A model for wetting and evaporation of a post-blink precorneal tear film', *Math. Med. Biol.* **27**, 211–225.

Wong, H., Fatt, I. and Radke, C. J. (1996), 'Deposition and thinning of the human tear film', *J. Coll. Interface Sci.* **184**, 44–51.

Zubkov, V., Breward, C. and Gaffney, E. (2012), 'Coupling fluid and solute dynamics within the ocular surface tear film: A modelling study of black line osmolarity', *Bull. Math. Biol.* **74**(9), 2062–2093.

Zubkov, V., Breward, C. and Gaffney, E. (2013), 'Meniscal tear film fluid dynamics near marx's line', *Bull. Math. Biol.* **75**, 1524–1543.